

S2. Configuration obtained from density functional theory

A minimum energy configuration of a TMC-MPD dimer was calculated using density functional theory (DFT) at the B3LYP/6-31G* level of theory as described in the main text to determine the values of the bond lengths in the amide bond and the amine and acyl chloride side groups. A protein database (.pdb) file of the final configuration is included in the accompanying files. Figure S2 shows a visualisation of the final configuration.

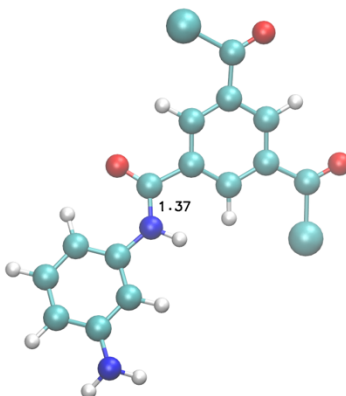


Figure S2: Visualisation of a relaxed TMC-MPD dimer obtained by DFT calculation. The length of the C-N amide bond is shown.

S3. Atomic structures of membranes described in the main text

Each computational cell produces two independent membranes due to the periodic boundary conditions applied and the setup of the simulation cell. In the main text we have exemplified this by showing an atomic structure of one of the two membranes formed at a particular composition. Figures S3 to S8 show snapshots of the atomic structures of all six membranes in these computational cells.

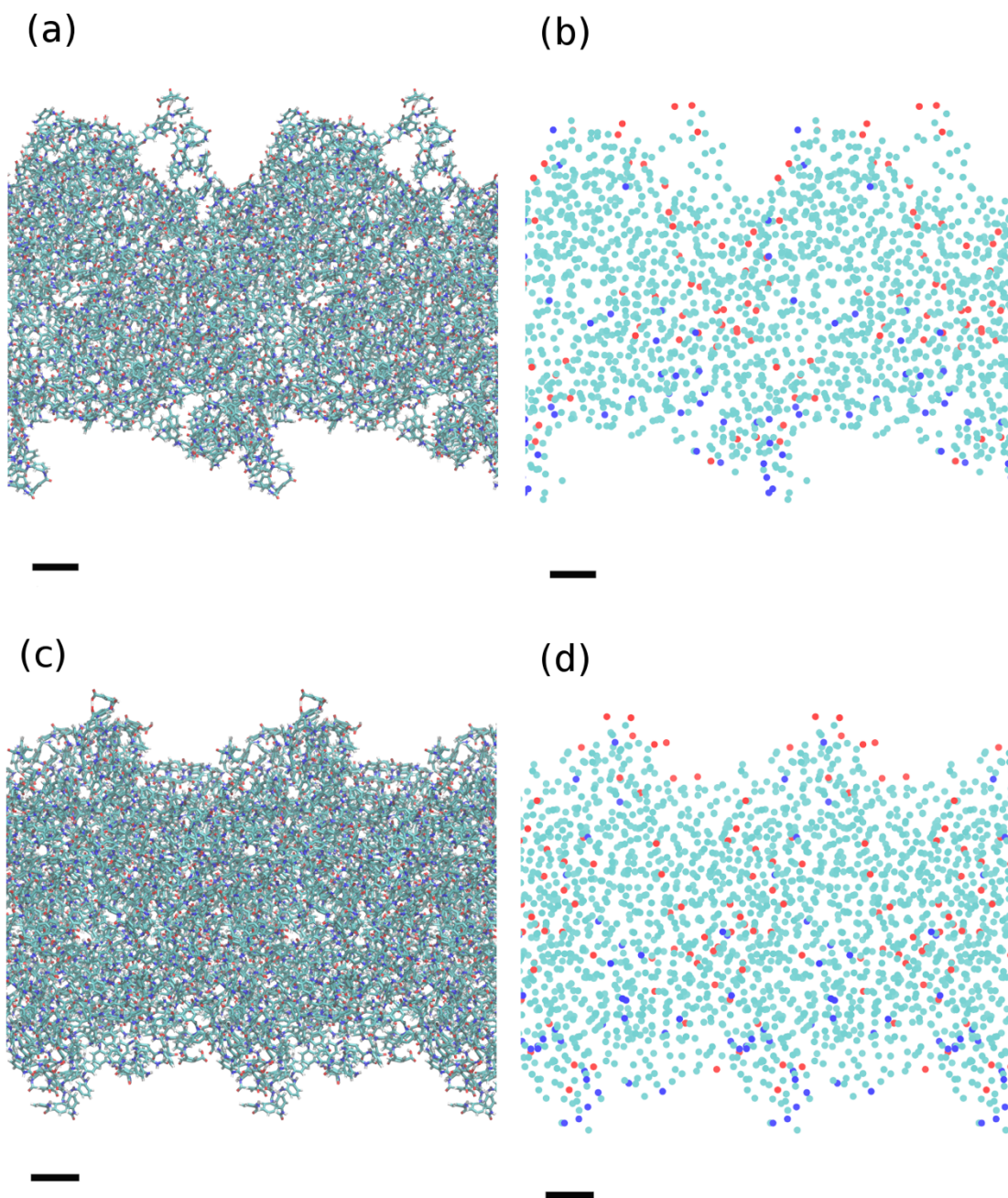


Figure S3 (Figure 7 in the main text) : One of the two membranes formed in the computational cell with a 1:1 composition of MPD:TMC. (a) Projected atomic structure along x, where red dots are oxygen atoms and dark blue dots are nitrogen atoms. (b) The same view as in (a) but showing the nitrogen atoms in amide bonds (cyan), the oxygen atoms in the hydroxyls of the carboxyl groups (red) and the nitrogen atoms in the amine groups (dark blue). Carboxyl groups are assumed to be formed from the remaining acyl chloride groups when the membrane is exposed to water. (c) and (d) are the same as (a) and (b), but viewed along z. The scale bars show 1 nm.

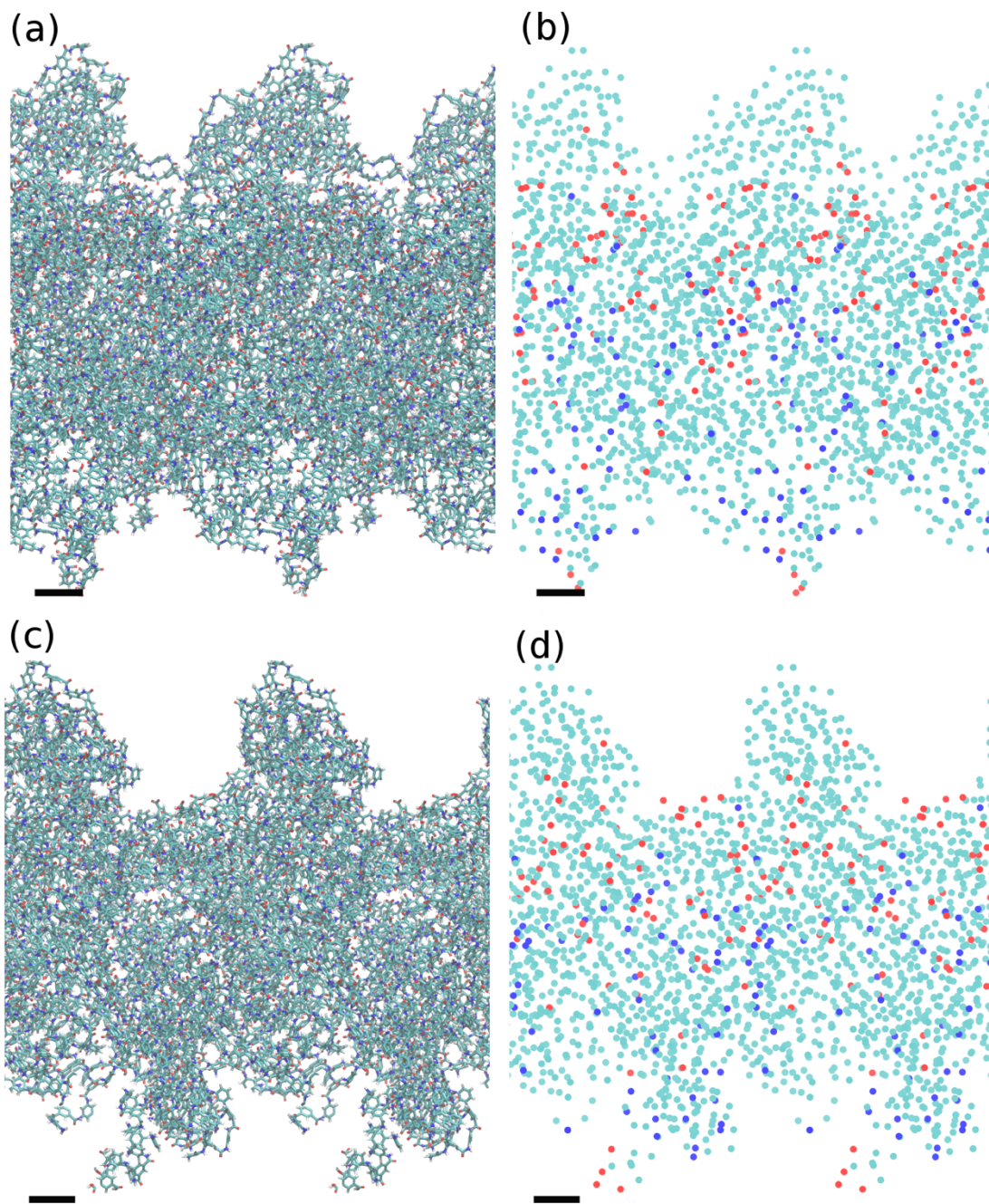


Figure S4: Second of the two membranes formed in the computational cell with a 1:1 composition of MPD:TMC. Other details as in caption of figure S3.

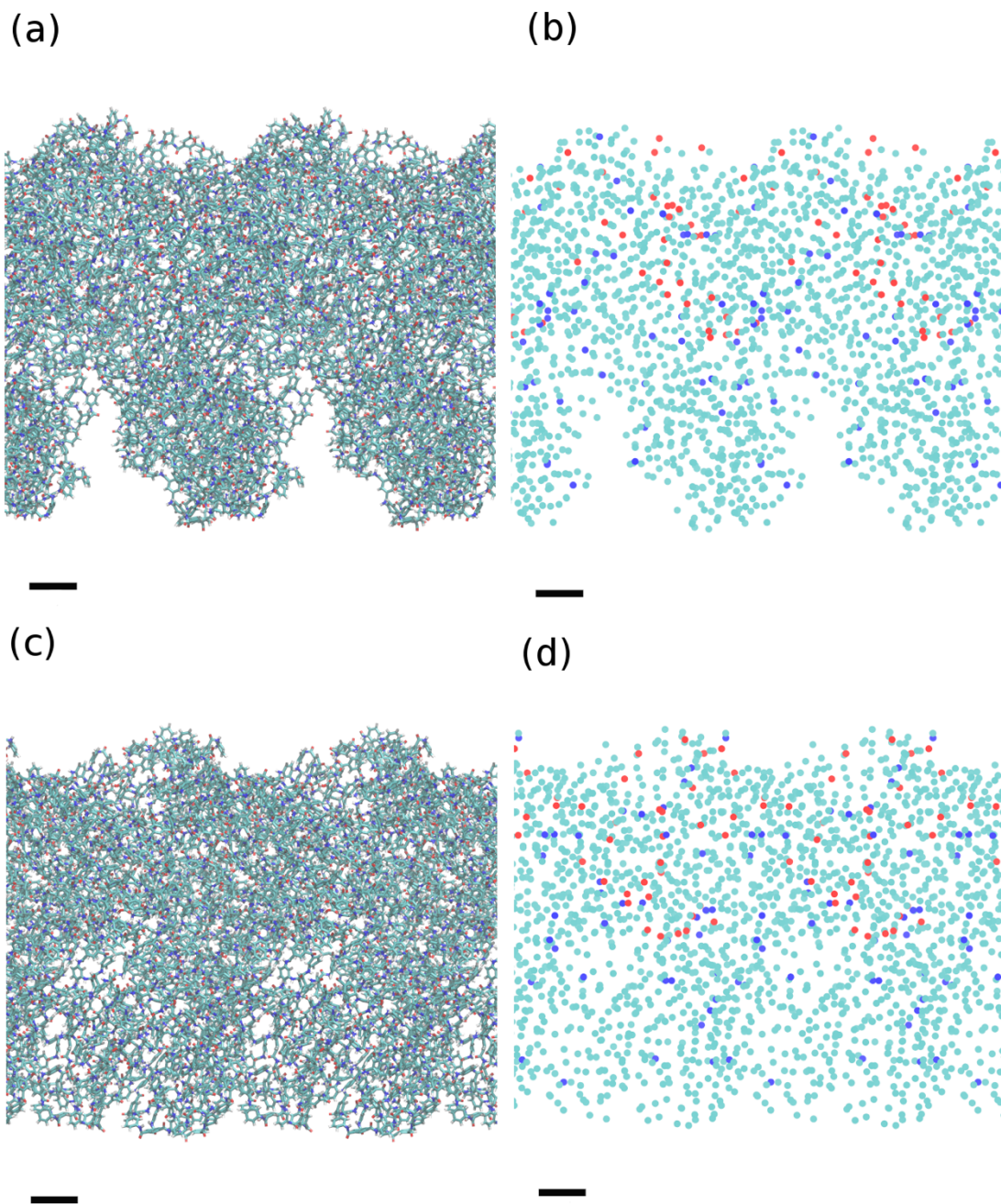
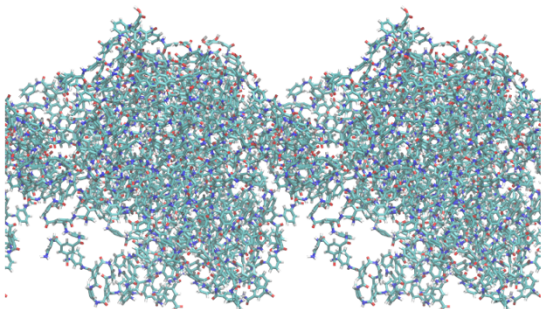
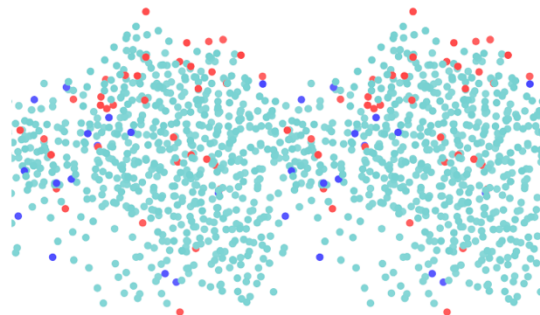


Figure S5: First of the two membranes formed in the computational cell with a 3:1 composition of MPD:TMC. Other details as in caption of figure S3.

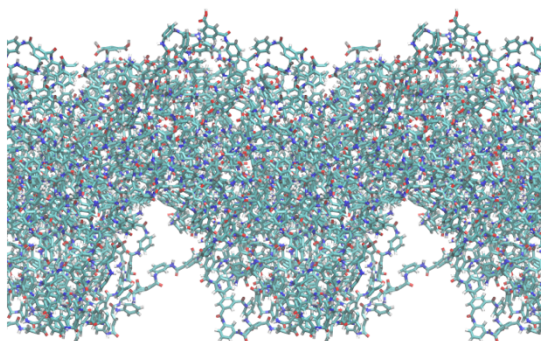
(a)



(b)



(c)



(d)

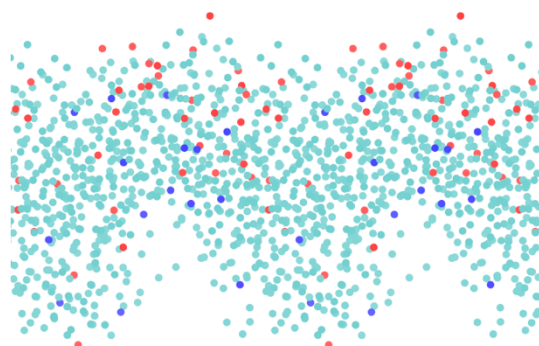


Figure S6: Second of the two membranes formed in the computational cell with a 3:1 composition of MPD:TMC. Other details as in caption of figure S3.

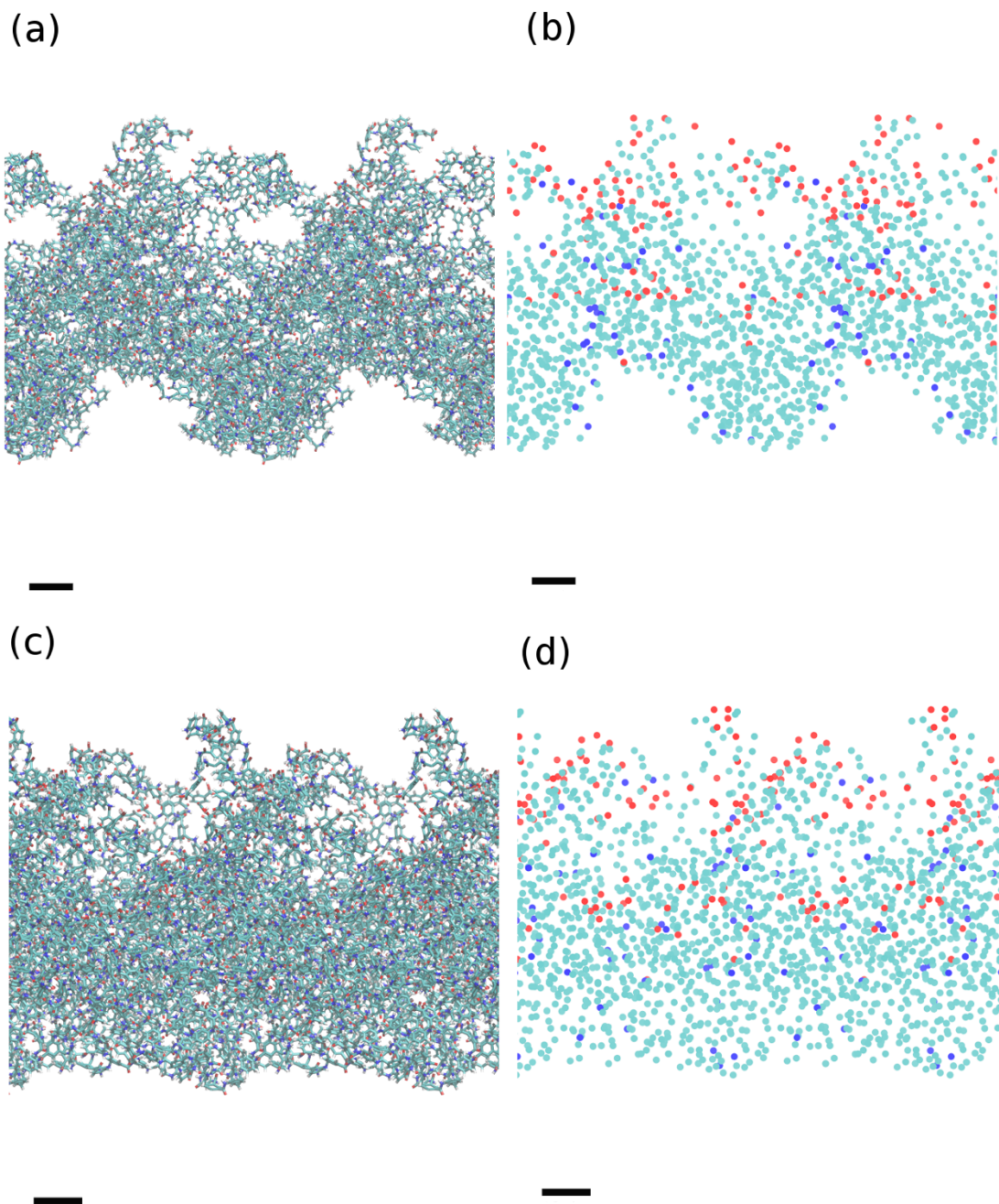


Figure S7: First of the two membranes formed in the computational cell with a 3:1 composition of MPD:TMC. Other details as in caption of figure S3.

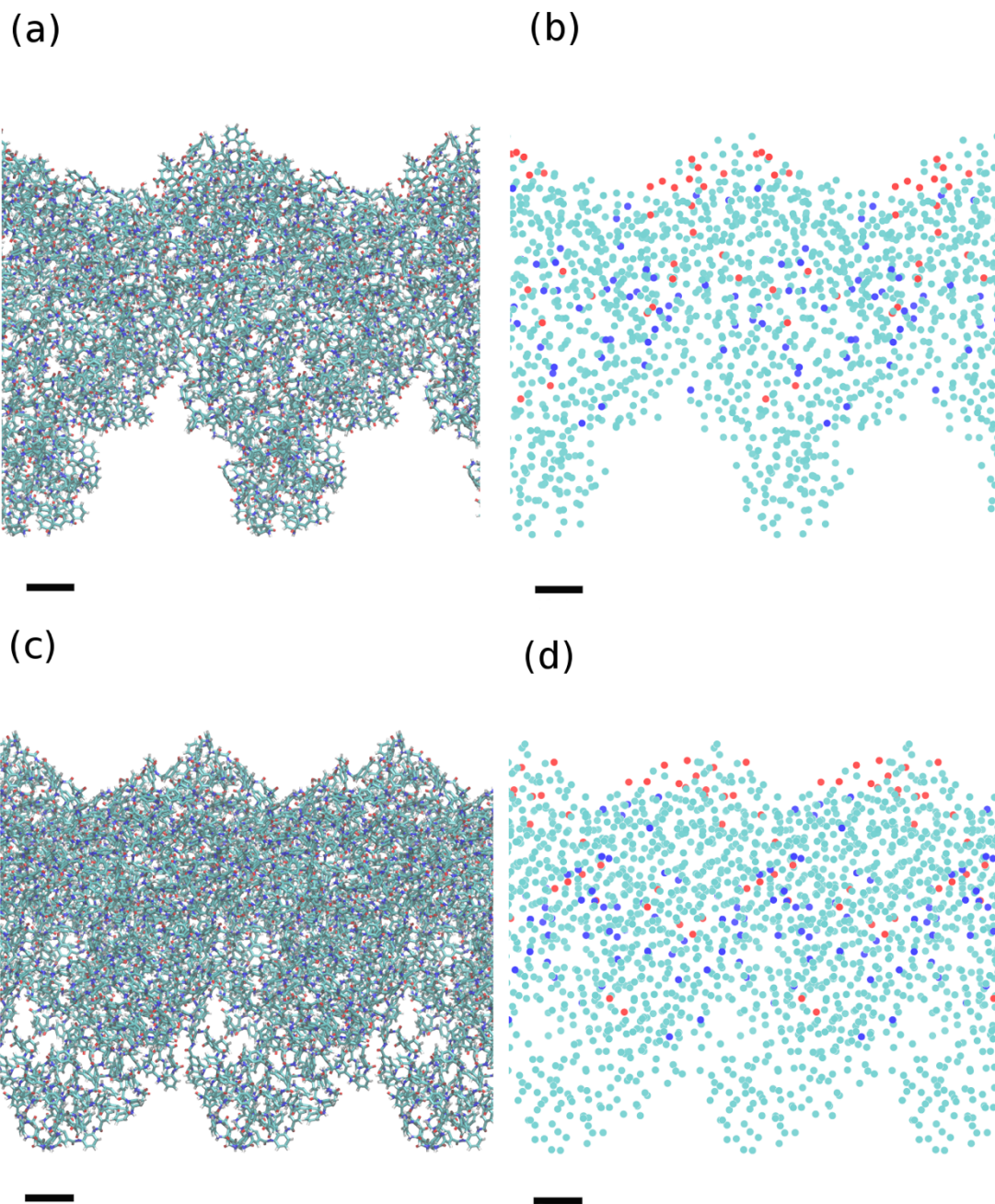


Figure S8: Second of the two membranes formed in the computational cell with a 3:2 composition of MPD:TMC. Other details as in caption of figure S3.

S4. The Amide Bond

As described in the main text, the amide bond should be coplanar with the bonds B_T-C and B_M-N connecting the carbon and nitrogen atoms to the two benzene rings, as shown in Fig. 3a. It is essential to maintain this coplanarity to avoid spurious polymerized configurations. The bond angles B_T-C-N and $C-N-B_M$ are approximated as 120° . The coplanarity could be achieved by introducing a $B_T-C-N-B_M$ torsion potential, but it would have to be supplemented by a bond-stretching potential to give the correct amide bond length.

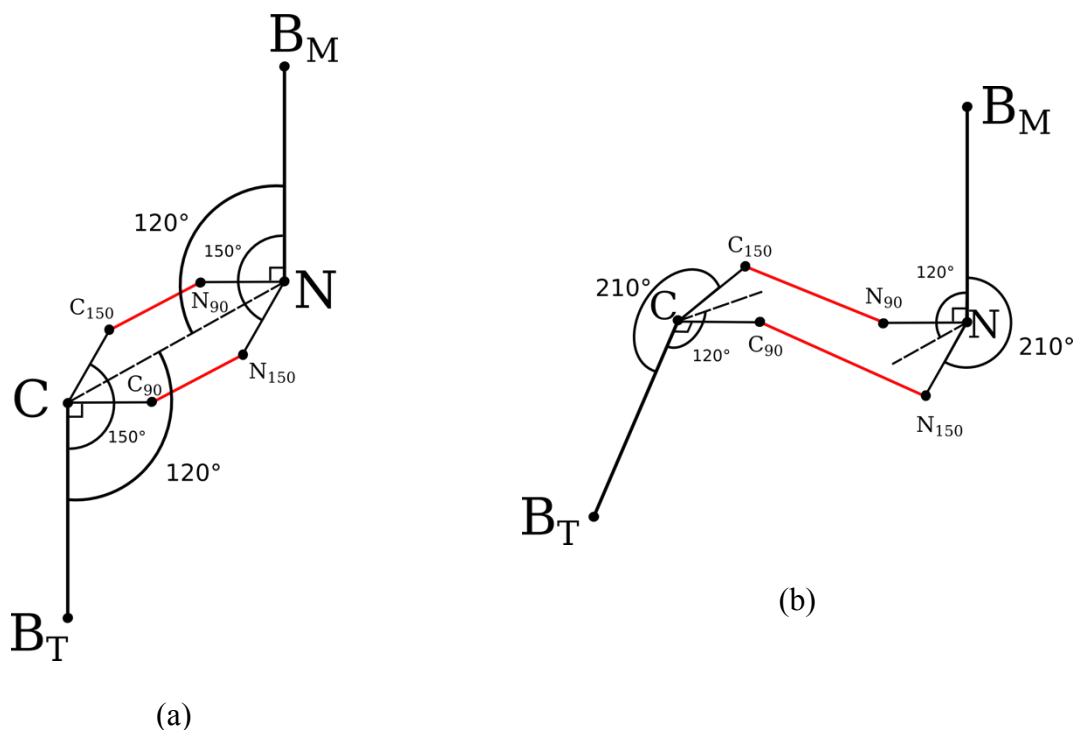


Figure S9: (a) The ground state of the amide bond in the coarse-grained representation. Sites B_T , C , N and B_M lie in the plane of the page. The $C-N$ bond is shown by the broken line. The red lines show harmonic bonds, also in the plane of the page, acting between fictitious sites C_{90} and N_{150} and between fictitious sites C_{150} and N_{90} . (b) To illustrate the location of fictitious sites C_{90} , C_{150} , N_{90} and N_{150} when bonds B_M-N and B_T-C are not coplanar. The red lines again show harmonic bonds to restore the correct bond length for the $C-N$ bond and coplanarity of sites B_T , C , N and B_M . The incipient amide bonds are shown by broken lines; they lie on the cones shown in Fig. 2 (main text). When the harmonic bonds are fully relaxed the broken lines are collinear and coincident with the $C-N$ bond

Instead, we have devised a simple procedure that simultaneously favours the coplanarity of $B_T-C-N-B_M$ and the correct length of the $C-N$ bond. The $C-N$ bond is modelled by two stiff harmonic bonds, as illustrated in red in Fig. S9a, which shows the planar equilibrium configuration. During

the simulation the bonds B_T-C and B_M-N are unlikely to be coplanar when the carbon and nitrogen atoms come within the range of 2.38 \AA for forming an amide bond. When this occurs, and as illustrated in Fig. S9b, two sites C_{90} and C_{150} are defined at 0.69 \AA from the carbon site, in the plane containing the B_T-C bond and the nitrogen atom, and at 90° and 150° respectively to the B_T-C bond. Similarly, sites N_{90} and N_{150} are defined at 0.69 \AA from the nitrogen site, in the plane containing the B_M-N bond and the carbon atom, and at 90° and 150° respectively to the B_M-N bond. To ensure an equilibrium C–N bond length of 1.375 \AA , s is set equal to $1.375 - 2 \times 0.69 \times \cos(30) = 0.18 \text{ \AA}$. The force constant is set to $100 \text{ kcal/mol/\AA}^2$ (4.336 eV/\AA^2) for each spring. This configuration enforces the coplanarity of the $B_T-C-N-B_M$ sequence, the correct length of the C–N bond, and bond angles B_T-C-N and $C-N-B_M$ of 120° .

S5. Non-bonded interactions

The non-bonding interaction, $U(r)$, between monomers is approximated by Lennard-Jones (LJ) potentials acting between the vertices, B, of the equilateral triangles representing benzene rings on different monomers,

$$U(r) = 4\varepsilon_{ij} \left[\left(\frac{\sigma_{ij}}{r_{ij}} \right)^{12} - \left(\frac{\sigma_{ij}}{r_{ij}} \right)^6 \right] \quad (\text{S1})$$

where r is the distance between centers of a pair of beads labeled i and j ; ε_{ij} is the depth of the potential-energy well, and σ is the length scale, corresponding to the distance where the potential changes from a repulsive to an attractive nature (roughly a segment diameter). At a distance larger than r_{cut} , the potential is fixed to zero. At long range monomers interact only through these LJ potentials. At short range these potentials are supplemented by purely repulsive Weeks-Chandler-Anderson (WCA) interactions between side groups of the same kind. The WCA model corresponds to a LJ cut to zero at a value of the potential minima (corresponding to $2^{1/6} \sigma$) and shifted positively by a value of ε . The potential is purely repulsive, but soft in nature so the simulation dynamics are not affected. WCA repulsive sites are put in place to avoid significant atomic overlap that might otherwise occur if the interactions between monomers of the same kind involved only LJ potentials between their benzene rings. The parameters for the non-bonding potentials are given in Table S1. The only interactions between unlike species are those between unlike side groups which lead to amide bonds, as described above. The mass of each coarse-grained monomer is the total mass of the monomer before polymerization occurs. The masses assigned to the interacting species in the coarse-grained model are also given in Table S1.

Table S1: Parameters for potentials and masses used in the coarse-grained modelling of monomer interactions. ϵ_{ii} and σ_{ii} are Lennard-Jones parameters between like species i , with radial cutoffs given by r_{cut} . Values for ϵ_{ii} are given in kcal/mol and for σ_{ii} and r_{cut} in Å. Masses are given in atomic mass units.

Species	ϵ_{ii}	σ_{ii}	r_{cut}	Mass
B	0.239	3.49	12.0	26
N	0.239	1.37	$2^{1/6} \sigma_{NN}$	3
C	0.239	1.37	$2^{1/6} \sigma_{CC}$	12
N ₉₀ /N ₁₅₀ (MPD)	-	-	-	6
C ₉₀ /C ₁₅₀ (TMC)	-	-	-	8

S6. Hydrated membrane density profiles

Density profiles are provided for all membranes described in figures S3-S8.

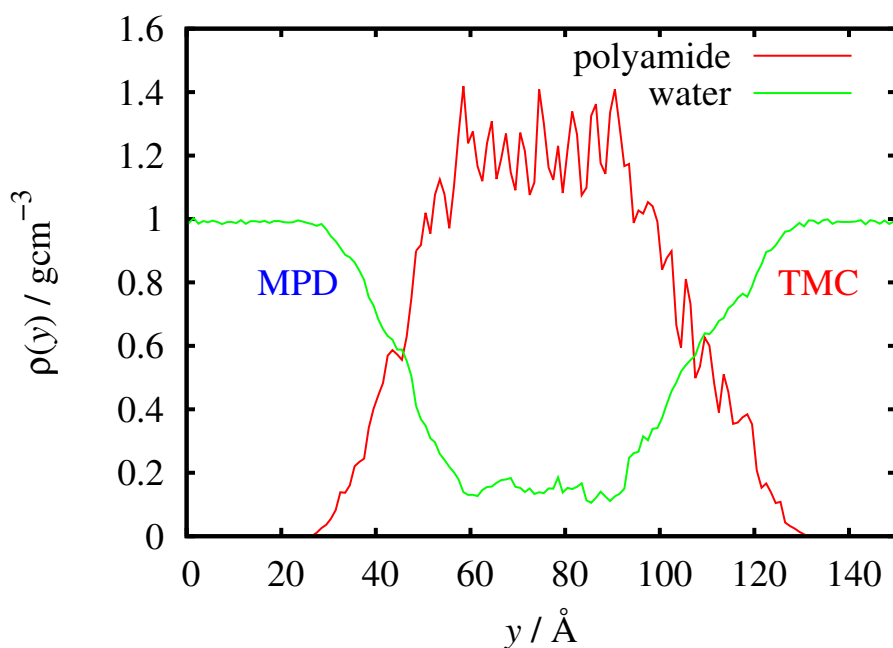


Figure S10 (Figure 9 in the main text) : Density along the transverse (z) direction for the first of the two membranes formed in the computational cell with a 1:1 composition of MPD:TMC.

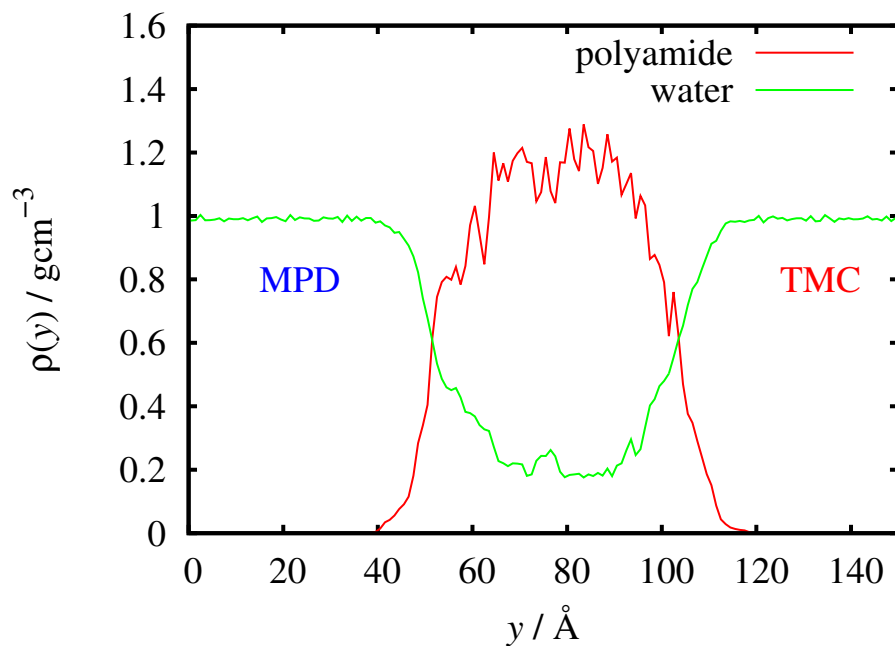


Figure S11 Density along the transverse (z) direction for the second of the two membranes formed in the computational cell with a 1:1 composition of MPD:TMC..

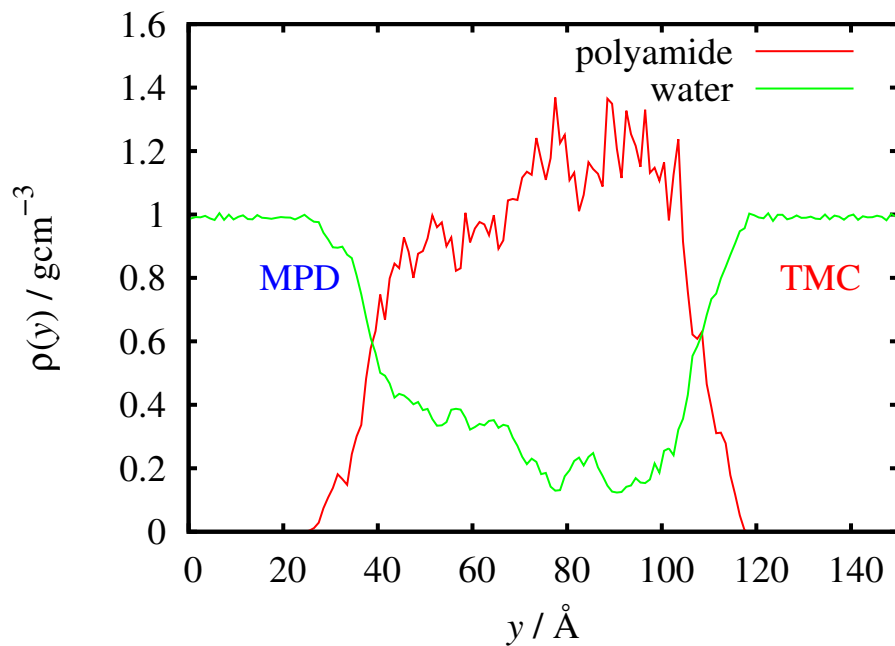


Figure S12 Density along the transverse (z) direction for the first of the two membranes formed in the computational cell with a 3:1 composition of MPD:TMC..

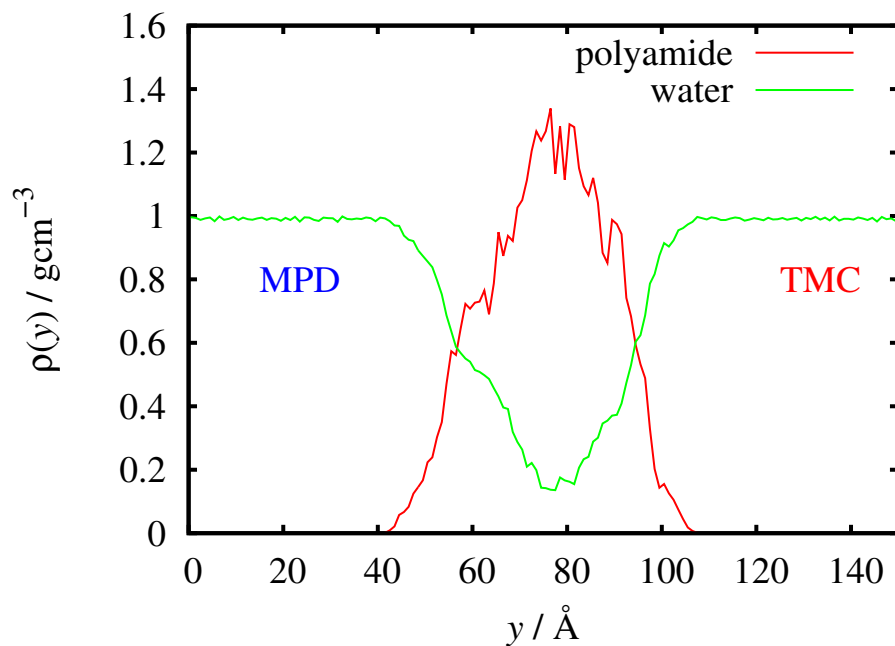


Figure S13 Density along the transverse (z) direction for the second of the two membranes formed in the computational cell with a 3:1 composition of MPD:TMC.

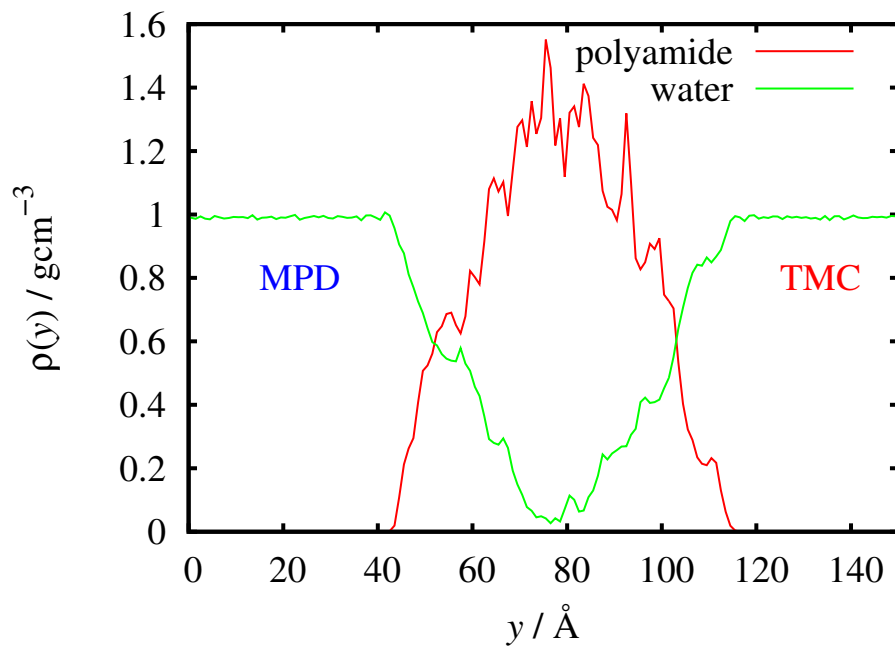


Figure S14 Density along the transverse (z) direction for the first of the two membranes formed in the computational cell with a 3:2 composition of MPD:TMC.

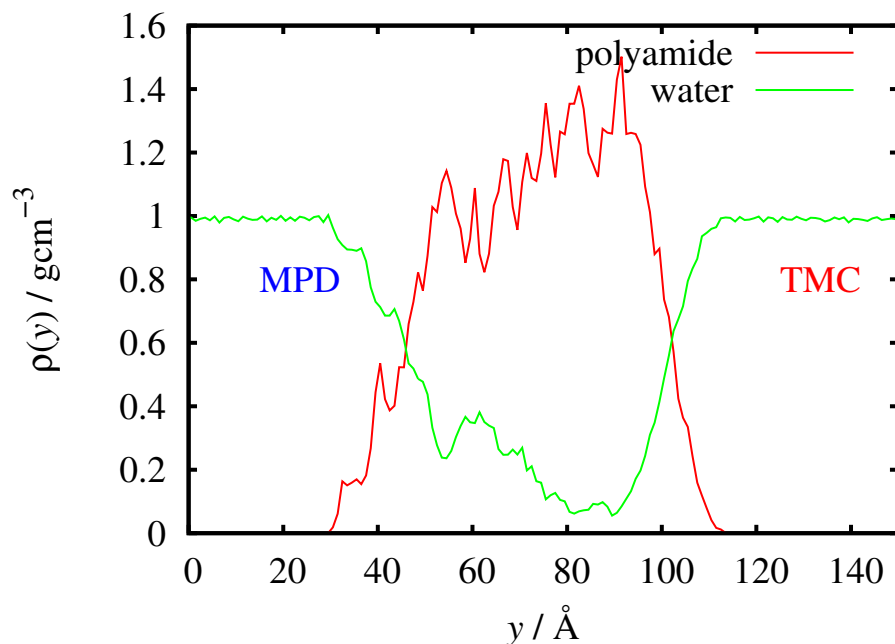


Figure S15 Density along the transverse (z) direction for the second of the two membranes formed in the computational cell with a 3:2 composition of MPD:TMC.

S5. Dry and hydrated densities

Average densities of dry and hydrated membrane conformations are given in Table S2. A region of 20-40 Å around the center of mass of the membrane in the y direction (*c.f.* Figures S10-15) is taken to average out the polymer densities.

Table S2: Polymer density (in g/cm^3) for dry and hydrated membranes. Membranes are characterized by the ratio of MPD:TMC used to form them. Each simulation produces two membranes, hence the two independent results. 1.30₆ corresponds to 1.30 \pm 0.06. Swelling corresponds to the change in volume upon hydration and is expressed in percentage (%). Uptake corresponds to the mass of water adsorbed expressed in percentage (%)

Membrane	Dry	Hydrated (water free)	Hydrated	Swelling	Uptake
1:1	1.30 ₆	1.22 ₅	1.37 ₄	5.3	12
1:1	1.27 ₈	1.17 ₄	1.35 ₄	3.8	15
3:1	1.16 ₁₃	1.15 ₁₂	1.36 ₅	13.4	18
3:1	1.33 ₅	1.28 ₈	1.37 ₄	8.9	7
3:1	1.28 ₈	1.13 ₁₂	1.37 ₄	7.7	21
3:1	1.17 ₈	1.15 ₉	1.37 ₅	7.2	19
Average	1.25 ₈	1.18 ₈	1.37 ₄	7.7	16

Hydrated membrane densities are reported including the trapped water and excluding it (water-free). Water uptake is calculated by taking the ratio of the hydrated density vs solvent-free density.

S6. Underlying data

Data underlying this article including input files and software used in this work, as well as final atomistic polyamide configurations can be accessed at

<http://dx.doi.org/10.6084/m9.figshare.3803688>,

and can be used under the Creative Commons Attribution licence.